Supplementary Information

Unraveling the Anion Storage Properties of Manganese doped $SrTiO_3$

Dushyant K. Sharma[1], Susanta S. Roy[1]*, Binson Babu[1]*

[1]*Department of Physics, School of Natural Science, Shiv Nadar Institution of Eminence, Uttar Pradesh-201314, India*

***Corresponding authors:** binson.babu@snu.edu.in, susanta.roy@snu.edu.in*

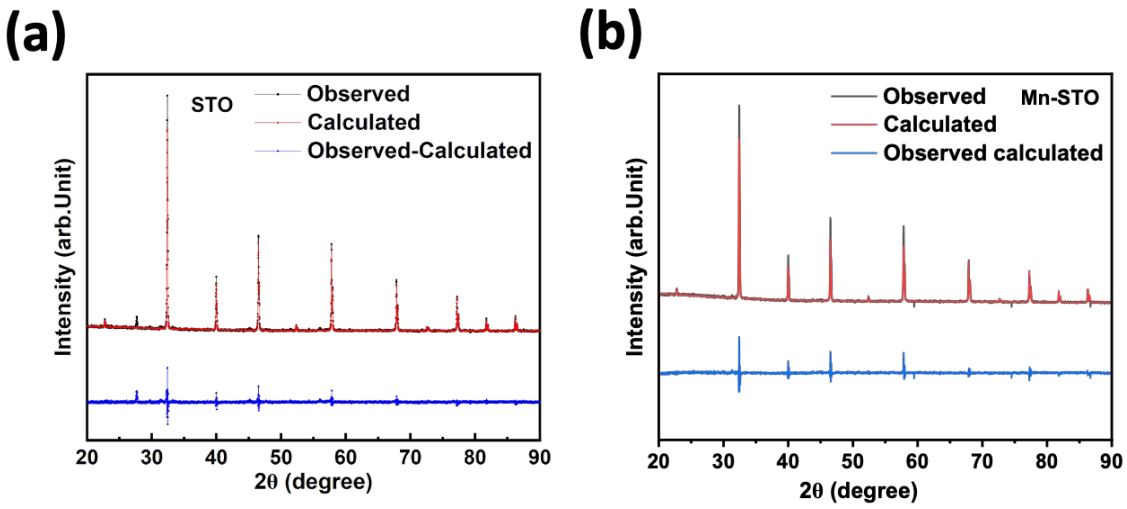

Figure S1. Rietveld refinement of (a) STO and (b) Mn- STO

- ## Calculation of Gold Schmidt tolerance factor

The Gold Schmidt tolerance factor (t) of perovskites is calculated by using the following equation,

$$t = \frac{R_a + R_o}{1.414(R_b + R_o)} \qquad \text{(S1)}$$

Where,

R_a = radius of the "a" cation.

R_b = radius of the "b" cation.

R_o = radius of the oxygen ion.

1) For STO**:**

R_a= Sr^{2+}=0.144 nm, R_b= Ti^{4+}=0.061 nm, R_o=R_o^{2-}=0.140 nm put these values in the equation 1.

$$t = \frac{0.144+0.140}{1.414\ (0.061+0.140)}$$

After solving this we get,

$$t = 0.999$$

2) For Mn-STO**:**

a) If Mn^{4+} replaces Ti^{4+} fully, then t factor $SrMnO_3$ will be
R_a= Sr^{2+}=0.144 nm, R_b= Mn^{4+}=0.053 nm, R_o=R_o^{2-}=0.140 nm put these values in the equation 1. It becomes perfect cubic.

$$t = \frac{0.144+0.140}{1.414\ (0.053+0.140)} = 1.041$$

b) If only 5% of Mn^{4+} replaces Ti^{4+}, then t factor $SrTi_{0.95}Mn_{0.05}O_3$ will be

R_a= Sr^{2+}=0.144 nm, $R_{eff} = 0.95 \times R_{Ti^{4+}} + 0.05 \times R_{Mn^{4+}} = 0.95 \times 0.061 + 0.05 \times 0.053 = 0.0606$

$$t = \frac{R_a + R_o}{1.414(R_{eff} + R_o)} = \frac{0.144 + 0.140}{1.414(0.0606 + 0.140)} = 1.001$$

Table S1. Structural parameters of STO and Mn-STO determined by Rietveld refinement.

STO	**Mn-STO**
a=3.904197	a=3.9016
Volume of unit cell=59.511 Å^3	Volume of unit cell=59.39 Å^3
R- factor =7.50	R- factor =7.69
χ^2 = 2.68	χ^2 = 2.25
R_{wp} = 15.31	R_{wp} = 28.2

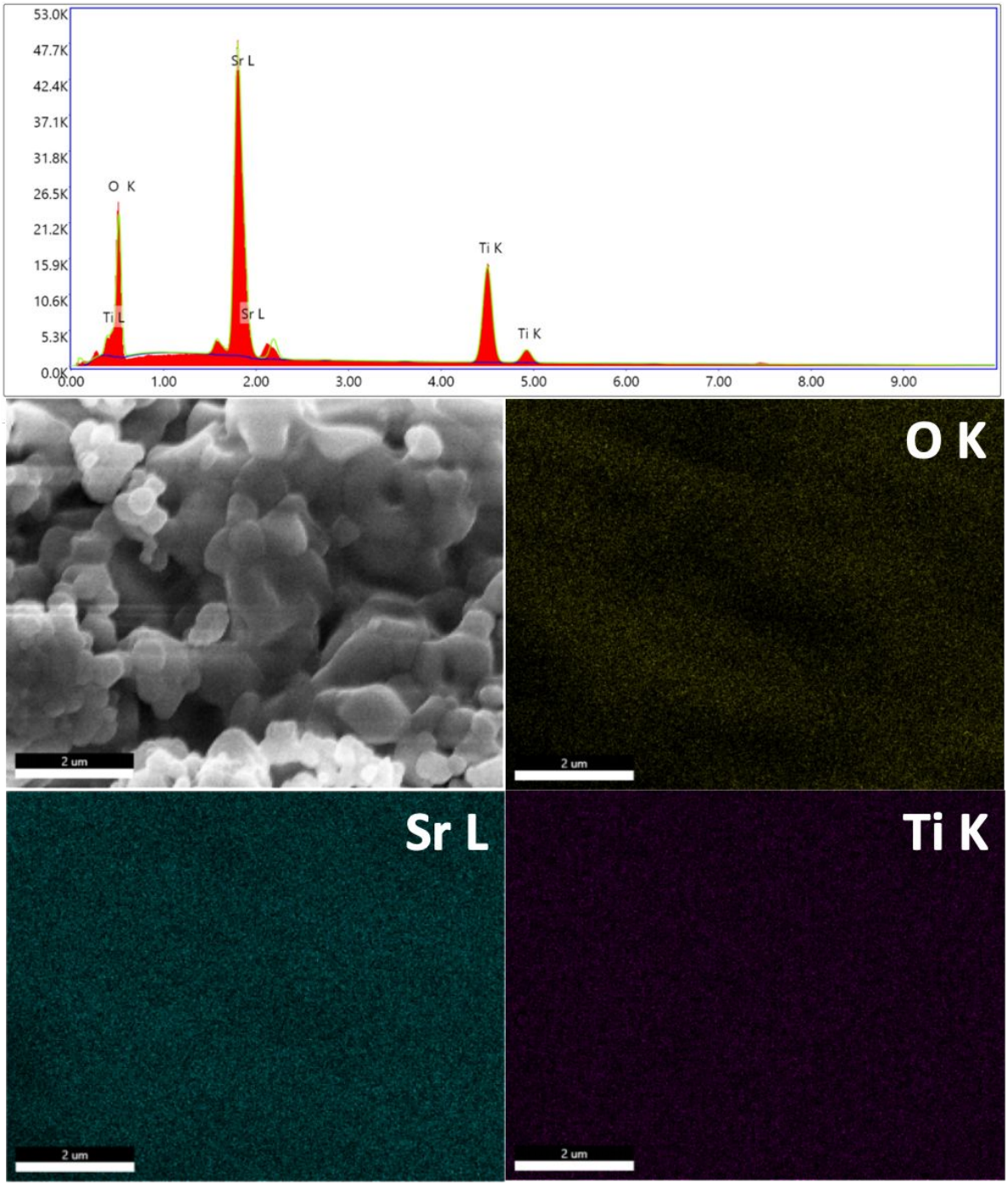

Figure S2. EDAX spectrum and elemental mapping of STO.

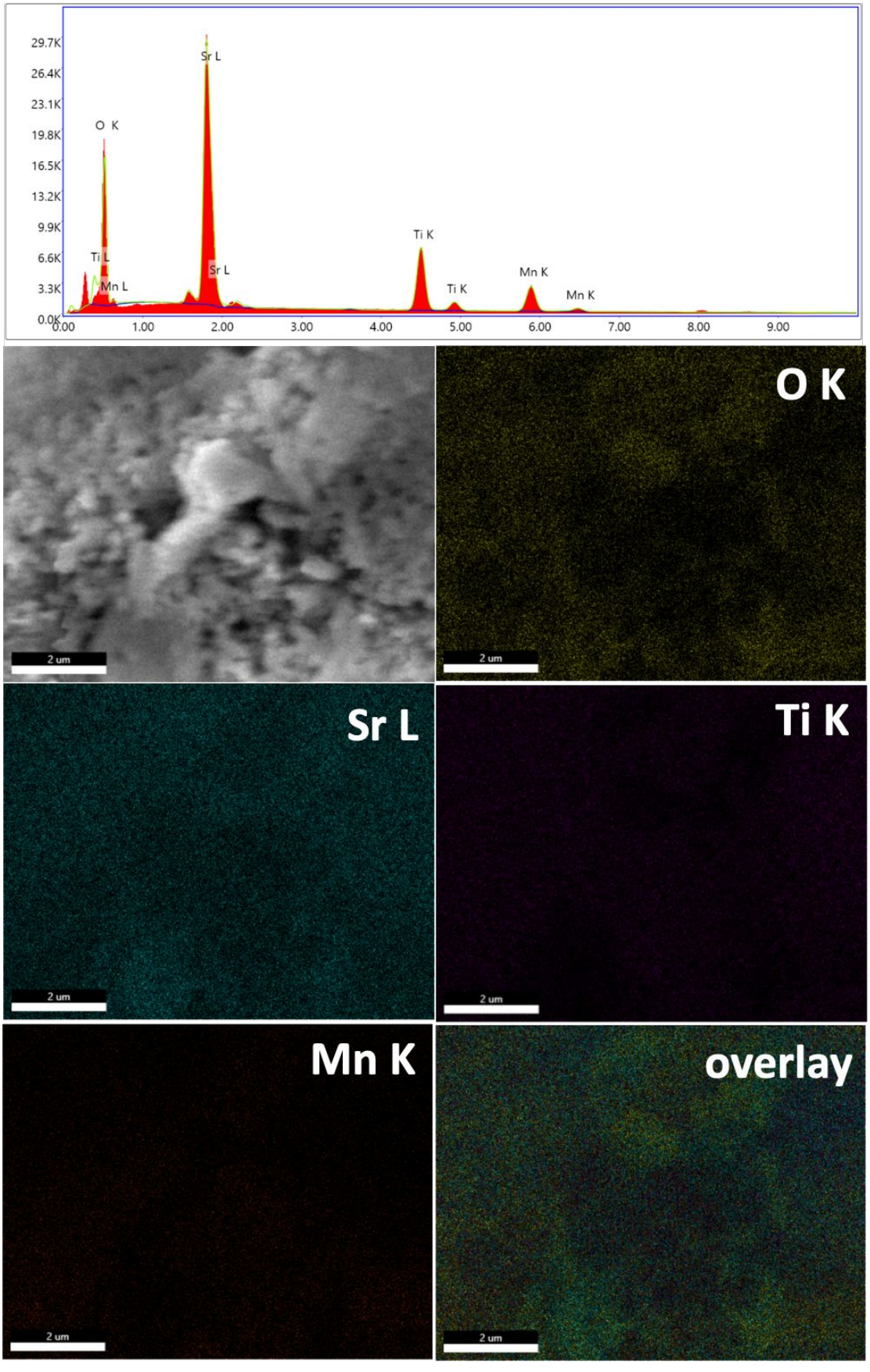

Figure S3. EDAX spectrum and elemental mapping of Mn-STO.

Table S2. Atomic percentage obtained from EDX spectroscopy for STO and Mn-STO.

STO	Atomic percentage (%)	Mn-STO	Atomic percentage (%)
Sr	44.14	Sr	23.06
Ti	25.44	Ti	20.64
O	30.41	O	43.59
		Mn	12.72

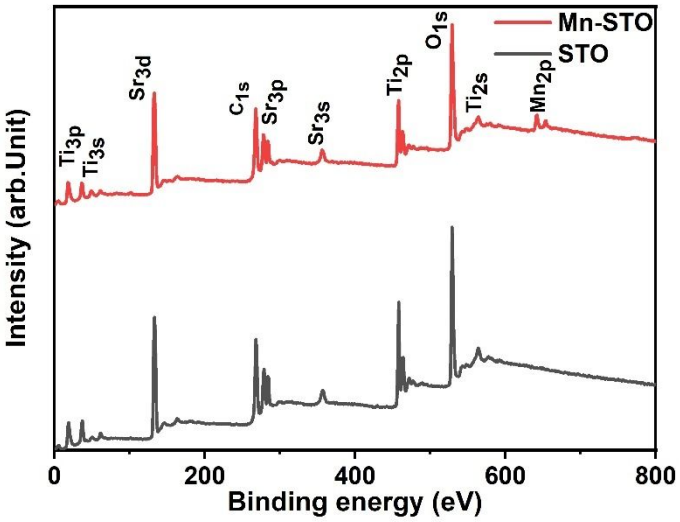

Figure S4. XPS Survey Scan of STO and Mn-STO.

Table S3. show the binding energy of STO and Mn-STO of XPS spectra.

Elements		STO (eV)	Mn-STO (eV)
Sr3d			
$Sr3d_{5/2}$		132.58	132.02
$Sr3d_{3/2}$		134.28	133.75
Ti2p			
$Ti2p_{3/2}$		457.99	457.58
$Ti2p_{1/2}$		463.61	463.28
O1s			
O^{2-}		529.12	528.70
$-OH/O_2$		530.04	530.27
Mn2p			
Mn2p3/2	Mn^{3+}	-	641.39
	Mn^{4+}		644.64
Mn2p1/2	Mn^{3+}	-	653.06
	Mn^{4+}		654.56

- **Calculation of electrochemical surface area (ECSA)**

We use Randle-Sevick's equation to calculate Electrochemical surface area (ECSA) of the electrode material. [1,2]

$$I_p = 2.68*10^{-5}\ n^{3/2}\ A\ D^{1/2}\ C\ v^{1/2} \qquad (S2)$$

where,

I_p = peak current

A = Area (Active area)

D = diffusion coefficient = $7.2*10^{-6}$

C = concentration of electrolyte (5mM) = $5*10^{-3}$ M

v = Scan rate (mVs^{-1})

n = no. of electrons, (n = 1)

After rearranging the equation (1)

$$\frac{I_P}{v^{0.5}} = 2.68*10^{-5}*1*7.2*10^{-6}*5*10^{-3}*A \qquad (S3)$$

Plot graph between scan rate V (mVs^{-1}) from different CV scans vs current I_p (mA)

Take the slope from the linear fitting of plot I_p vs $V^{0.5}$ from the anodic peak of the CV scan at different scan rates.

Hence,

$$A = \frac{Slope\ of\ I_p}{2.68*10^5*7.2*10^{-5}*5*10^{-3}*1} \qquad (S4)$$

Hence from equation (3) we can calculate the Electrochemical surface area.

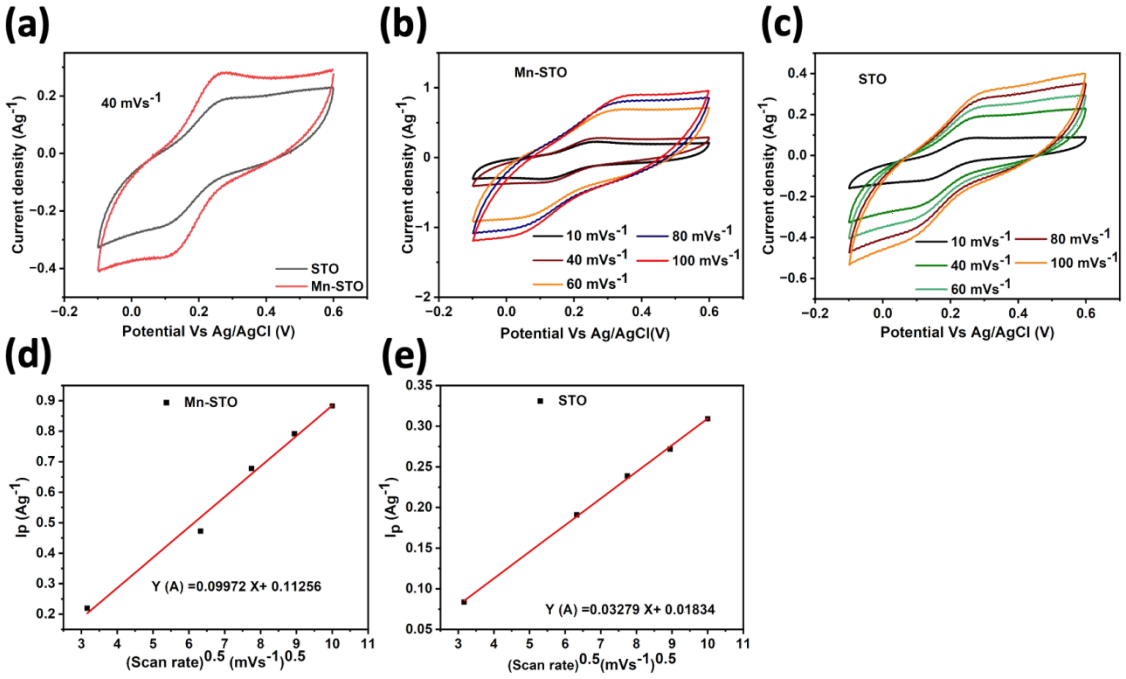

Figure S5. Cyclic voltammetry (a) comparing the STO and Mn-STO at 40 mV s^{-1}, at different scan rates for (b) Mn-STO and (c) STO using standard redox-active electrolyte 0.1 M KCl containing $5*10^{-3}$ M $Fe(CN)^{3-/4-}$, (d) and (e) displays the linear fitting of the Mn-STO and STO for finding the slope to calculate the electrochemical active surface area using Randle-Sevick's equation.

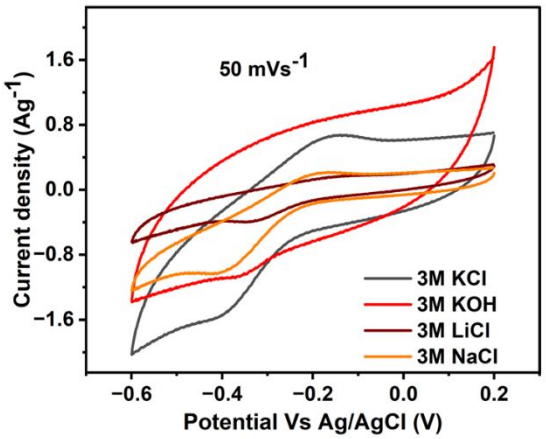

Figure S6. Comparison of cyclic voltammetry of pristine STO at 50 mVs^{-1} in different electrolytes.

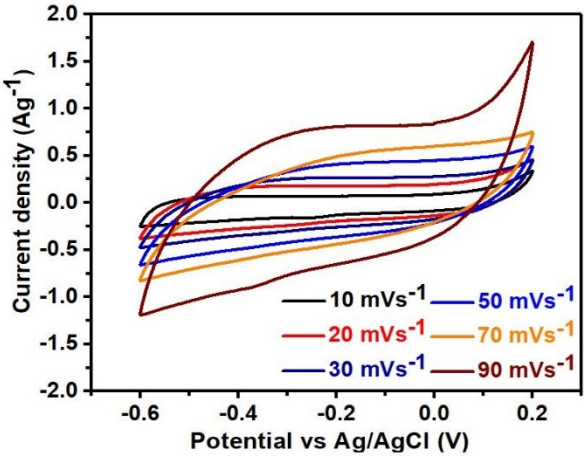

Figure S7. Cyclic voltammogram of STO at different scan rates in 3M KOH aqueous solution using the three-electrode setup

- ## Calculation of b value:

The energy storage mechanism can be calculated by using the CV scans at different scan rates according to the following power law[3–5]

$$i = av^b \qquad \text{(S5)}$$

Where,

i is the scan rate-dependent current.

v is the scan rate (mVs^{-1})

a and b are the adjustable parameters.

b is close to 1 signifies the current is capacitive in nature.

b is close to 0.5 signifying the diffusion-controlled phenomenon.

To determine the b values, log (i) vs. log (v) was plotted for different constant potentials and the slope of the best linear fit data provides the "b" value for each potential for the cathodic and anodic scan respectively.

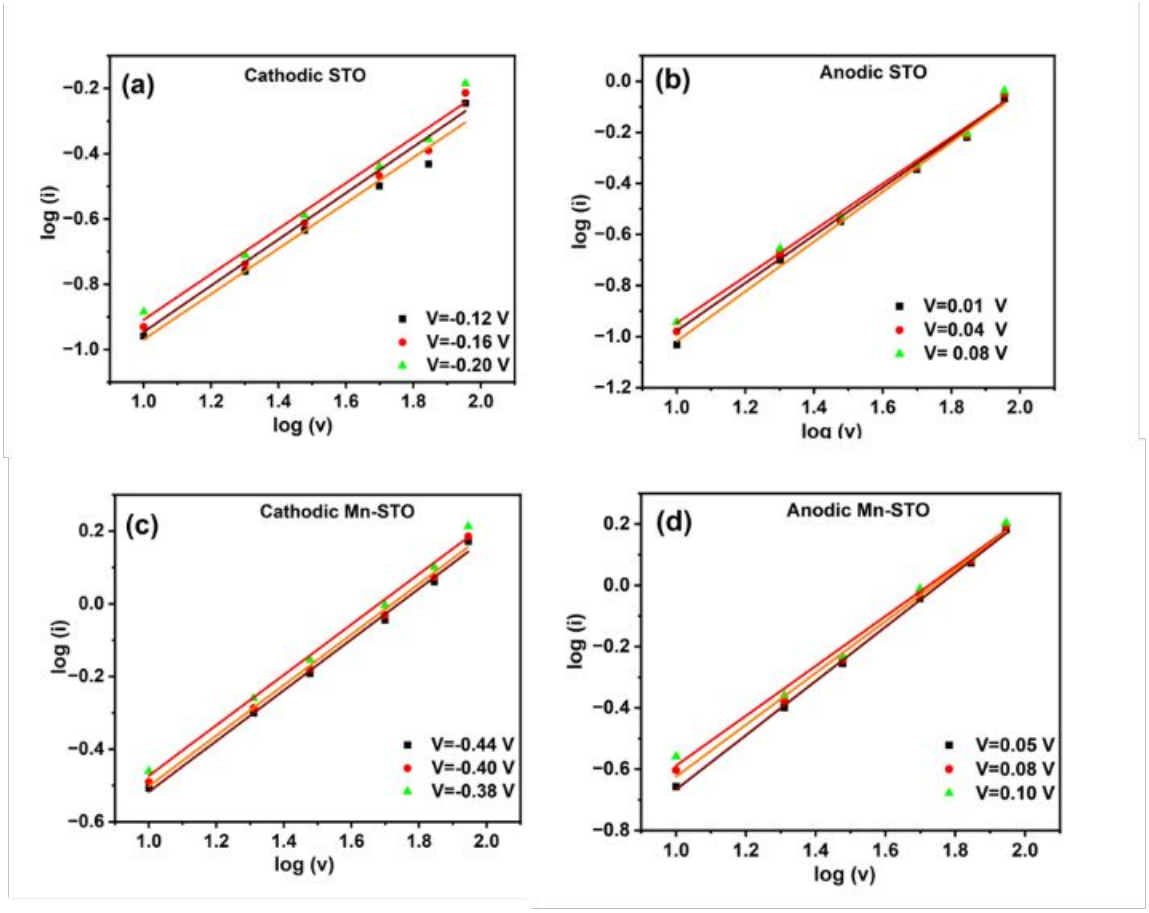

Figure S8. (a, b, c, d) log i" vs "log v" plot for STO and Mn-STO respectively. Plot showing the linear relationship of (a, c) cathodic (b, d) anodic sweep of cyclic voltammogram at the different potential.

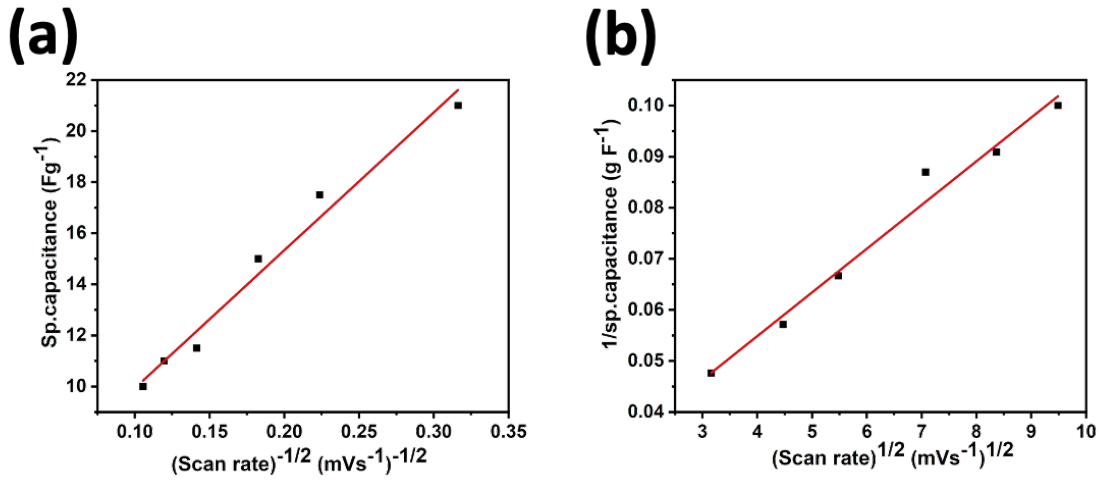

Figure S9. Trasatti's method for STO electrode for (a) specific capacitance *vs*. inverse of scan rate and (b) inverse specific capacitance *vs*. square root of scan rate.

- **Calculation of diffusion and non-diffusion controlled current contribution:**

To obtain the electrochemical kinetics of charge storage in the material the respective contributions are quantitatively distinguished, as diffusion and non-diffusion limited component.[6–8]

$$I(V) = K_1 v + K_2 v^{1/2} \qquad (S6)$$

Where,

$K_1 v$ = are the current contributions due to non-diffusion charge storage.

$K_2 v^{1/2}$ = diffusion-controlled intercalation processes.

v = scan rate.

By rearranging the equation. (5), we get

$$\frac{I(v)}{v^{0.5}} = k_1 v^{0.5} + K_2 \qquad (S7)$$

Plot graph between $\frac{I(v)}{v^{0.5}}$ vs $v^{0.5}$, from the linear fit of the graph, Slope and intercept of the straight line will give the value of K_1 and K_2 respectively. After finding the values

of K_2 at constant potentials V. Suppose we are taking the scan rate at 30 mVs^{-1} take current and voltage as x-axis and y-axis respectively.

Plot the graph between

X_1 = value of different constant voltage

Y_1 = K_2 values at different constant voltage.

X_2 = Voltage vs Ag/AgCl (V) | At 10 mVs^{-1}

Y_2 = Current density (Ag^{-1})

After plotting shaded region tells about "non- diffusion controlled" charge storage and from that we can easily calculate percentage of diffusion and non-diffusion controlled the charge storage.

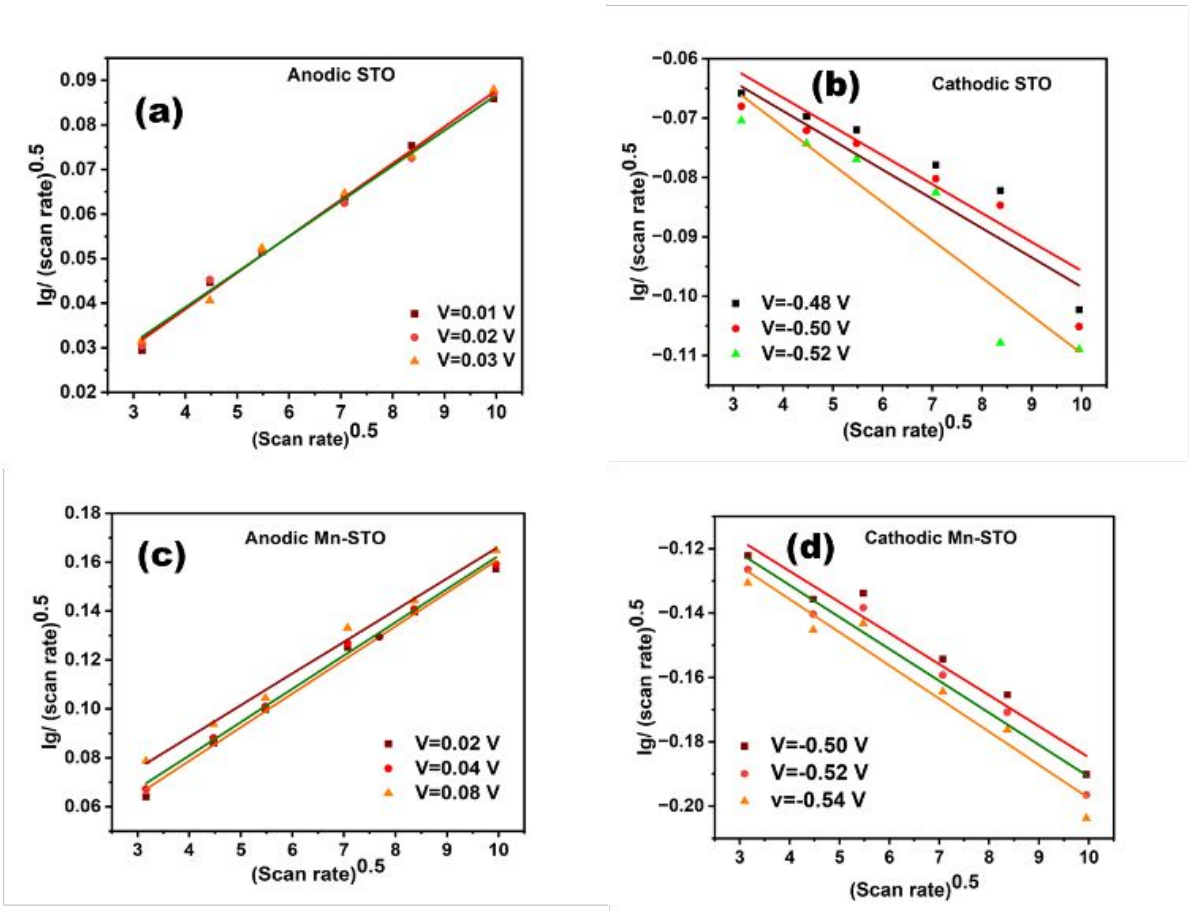

Figure S10. (a, b, c, d) (scan rate)$^{0.5}$ vs I_g/ (scan rate)$^{0.5}$ plot for STO and Mn-STO respectively. The slope and intercept of the straight line provide the values of K_1 and K_2. The plot displays the linear relationship of (a ,c) anodic and (b, d) cathodic sweep of cyclic voltammogram at different potentials.

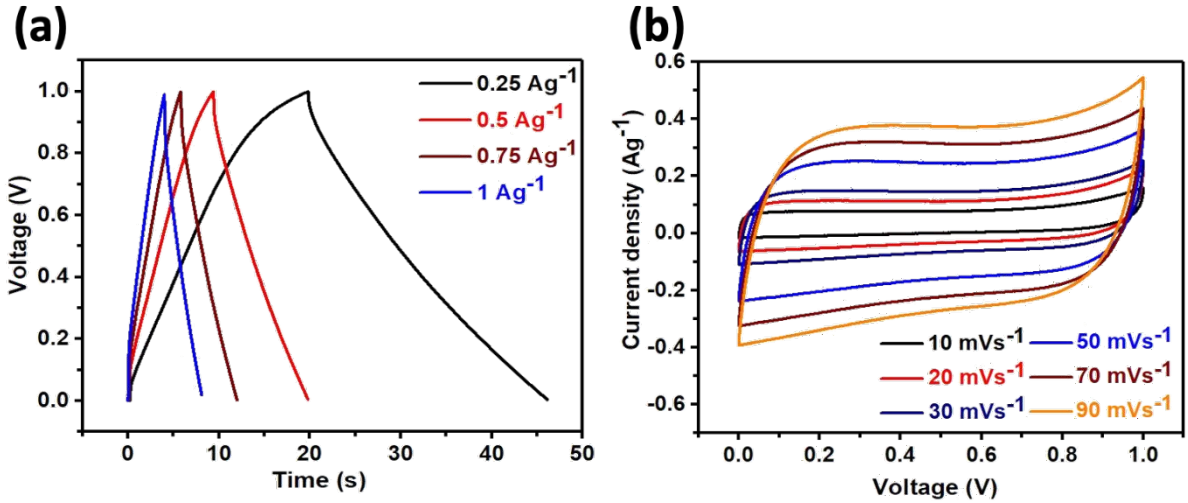

Figure S11. (a) galvanostatic charge-discharge at different current densities and (b) cyclic voltammogram at different scan rates of STO symmetric device in 3M KOH electrolytes.

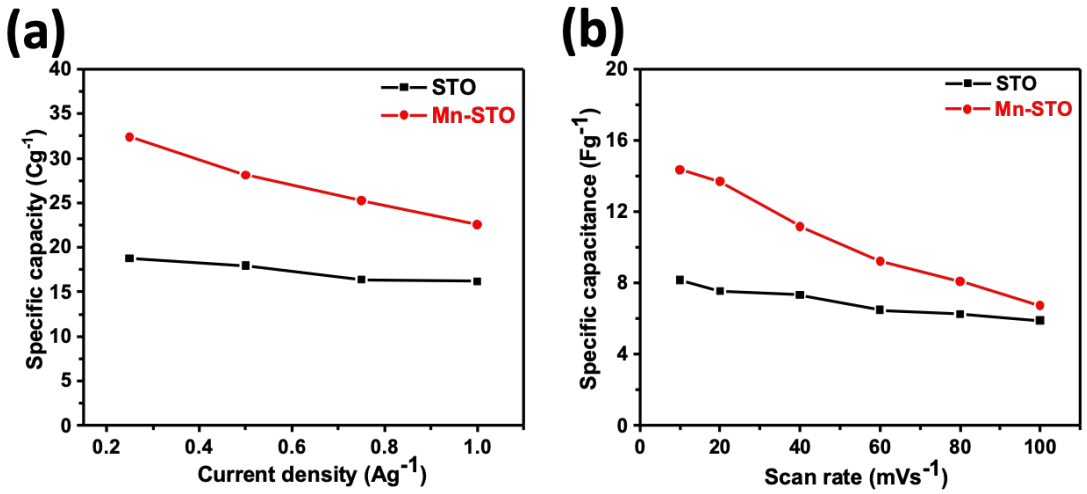

Figure S12. Comparison of (a) specific capacity and (b) specific capacitance calculated from the galvanostatic charge-discharge at different current densities and the cyclic voltammetry at different scan rates respectively.

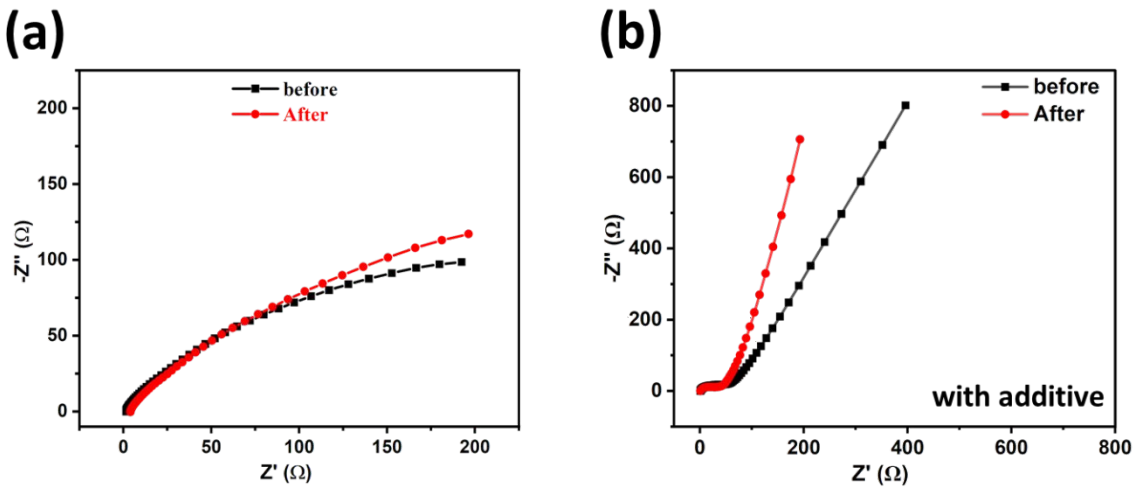

Figure S13. The Nyquist plot taken from the electrochemical impedance spectroscopy before and after the cycling stability at a current density of 1.0 A g-1 of Mn-STO symmetric cell (a) without adding additive and (b) with adding additive 0.1M $MnSO_4$ in aqueous 3M KOH electrolyte.

References

(1) Sharma, D. K.; Sain, S.; Maity, G.; Thomas, A.; Kumar, R.; Dhar, S.; Arora, H. S.; Babu, B.; Roy, S. S. Electrochemical Studies on Chromium Doped SrTiO3 for Supercapacitor Applications. *Nano Trends* **2024**, *6*, 100036. https://doi.org/10.1016/j.nwnano.2024.100036.

(2) Allen J. Bard, L. R. F. *Electrochemical Methods: Fundamentals and Applications, 2nd Edition*, 2nd ed.; John Wiley & Sons: New York, 2001.

(3) Babu, B.; Shaijumon, M. M. Studies on Kinetics and Diffusion Characteristics of Lithium Ions in TiNb2O7. *Electrochim. Acta* **2020**, *345*, 136208. https://doi.org/10.1016/j.electacta.2020.136208.

(4) Babu, B.; Ullattil, S. G.; Prasannachandran, R.; Kavil, J.; Periyat, P.; Shaijumon, M. M. Ti3+ Induced Brown TiO2 Nanotubes for High Performance Sodium-Ion Hybrid Capacitors. *ACS Sustainable Chem. Eng.* **2018**, *6* (4), 5401–5412. https://doi.org/10.1021/acssuschemeng.8b00236.

(5) Augustyn, V.; Come, J.; Lowe, M. A.; Kim, J. W.; Taberna, P.-L.; Tolbert, S. H.; Abruña, H. D.; Simon, P.; Dunn, B. High-Rate Electrochemical Energy Storage through Li+ Intercalation Pseudocapacitance. *Nat. Mater.*, **2013**, *12* (6), 518–522. https://doi.org/10.1038/nmat3601.

(6) Babu, B.; Shaijumon, M. M. Understanding How Degree of Crystallinity Affects Electrochemical Kinetics of Sodium-Ion in Brown TiO2 Nanotubes. *ChemElectroChem* **2021**, *8* (12), 2180–2185. https://doi.org/10.1002/celc.202100047.

(7) Babu, B.; Shaijumon, M. M. High Performance Sodium-Ion Hybrid Capacitor Based on Na2Ti2O4(OH)2 Nanostructures. *J. Power Sources* **2017**, *353*, 85–94. https://doi.org/10.1016/j.jpowsour.2017.03.143.

(8) Augustyn, V.; Simon, P.; Dunn, B. Pseudocapacitive Oxide Materials for High-Rate Electrochemical Energy Storage. *Energy Environ Sci.* **2014**, *7* (5), 1597–1614. https://doi.org/10.1039/C3EE44164D.